Title: Correction of autoimmune *IL2RA* mutations in primary human T cells using non-viral genome targeting

Authors: Theodore L. Roth[1,2,3,4,5], Ruby Yu[3,4,5], Eric Shifrut[3,4,5], Joseph Hiatt[1,2,3,4,5], Han Li[6,7], Kathrin Schumann[3,4,5], Victoria Tobin[3,4,5], Andrea M. Ferris[8], Jeff Chen[9], Jean-Nicolas Schickel[9], Laurence Pellerin[10], David Carmody[11], Gorka Alkorta-Aranburu[12], Daniela Del Gaudio[12], Min Cho[13], Hiroyuki Matsumoto[14], Montse Morell[15], Ying Mao[15], David Nguyen[3,4,5], Rolen Quadros[16], Channabasavaiah Gurumurthy[16], Baz Smith[15], Michael Haugwitz[15], Stephen H. Hughes[8], Jonathan Weissman[6,7], Andrew P. May[13], Gary Kupfer[17], Siri Greeley[11], Rosa Bacchetta[10], Eric Meffre[9], Maria Grazia Roncarolo[10], Neil Romberg[18], Kevan C. Herold[19], Manuel D. Leonetti[6,7], Alexander Marson[3,4,5,13,20,21] *

Affiliations:

[1] Medical Scientist Training Program, University of California, San Francisco, CA 94143, USA.

[2] Biomedical Sciences Graduate Program, University of California, San Francisco, CA 94143, USA.

[3] Department of Microbiology and Immunology, University of California, San Francisco, CA 94143, USA.

[4] Diabetes Center, University of California, San Francisco, CA 94143, USA.

[5] Innovative Genomics Institute, University of California, Berkeley, CA 94720, USA.

[6] Department of Cellular and Molecular Pharmacology, University of California, San Francisco, San Francisco, CA 94158, USA.

[7] Howard Hughes Medical Institute.

[8] HIV Dynamics and Replication Program, Vector Design and Replication Section, National Cancer Institute, Frederick, MD, 21702.

[9] Department of Immunobiology, Yale University School of Medicine, New Haven, CT.

[10] Division of Stem Cell Transplantation and Regenerative Medicine at Stanford University, and Department of Pediatrics, Institute for Stem Cell Biology and Regenerative Medicine, Stanford University, Stanford, CA.

[11] Section of Adult and Pediatric Endocrinology, Diabetes, and Metabolism, Department of Medicine, The University of Chicago, Chicago, IL, USA.

[12] Department of Human Genetics, The University of Chicago, Chicago, IL, USA.

[13] Chan Zuckerberg Biohub, San Francisco, CA 94158, USA.

[14] Takara Bio Japan.

[15] Takara Bio USA, Inc.

[16] Mouse Genome Engineering Core Facility, Vice Chancellor for Research Office, University of Nebraska Medical Center, Omaha, NE, USA.

[17] Department of Pediatrics, Pathology, Yale University School of Medicine, New Haven, CT.

[18] Department of Pediatrics, Children's Hospital of Philadelphia, Philadelphia, Pennsylvania.

[19] Departments of Immunobiology and Internal Medicine, Yale University, New Haven, CT.

[20] Department of Medicine, University of California, San Francisco, CA 94143, USA.

[21] UCSF Helen Diller Family Comprehensive Cancer Center, University of California, San Francisco, CA 94158.

* Correspondence to: alexander.marson@ucsf.edu

Abstract:

The full promise of cell-based immunotherapies depends on technology to engineer and correct targeted genome sequences in primary human immune cells. CRISPR-Cas9 genome editing components can be electroporated into primary cells for gene knock-out. To date, co-delivery of oligodeoxynucleotide homology-directed repair (HDR) templates has enabled the replacement of short stretches of nucleotides; however efficient delivery of longer HDR templates has required viral-encoded templates, limiting adaptability and therapeutic applications. Here, we describe methods for non-viral T cell genome targeting with Cas9 RNPs and long (>1 kilobase) non-viral HDR templates. Targeting was efficient across multiple blood donors and genomic loci, cell viability was high, and the procedure could be multiplexed for bi-allelic or multi-gene targeting. Long single-stranded (ss)DNA HDR templates limited observed off-target integrations using either Cas9 or a Cas9 "nickase." We were able to identify the causal mutations in *IL2RA* (interleukin-2 receptor alpha; *CD25*) in multiple siblings with monogenic autoimmunity and correct the mutations in their affected primary T cells. Non-viral genome targeting will allow rapid and flexible experimental manipulation of primary human immune cells and therapeutic engineering of patient cells.

One Sentence Summary: We developed non-viral methods to engineer long genome sequences in human T cells, enabling functional studies and correction of autoimmune mutations in patient cells.

Main Text:

Human T cells can be purified from blood, engineered *ex vivo*, and then returned to circulation through autologous transplantation. Engineered T cells are being developed to treat cancer and infectious diseases (*1*, *2*). These cell-based treatments depend on the ability to genetically reprogram T cells, for example to enhance their ability to recognize and attack specific antigens (*3*). Cell-based therapies involving modified regulatory T cells (Tregs) designed to suppress inflammation are being developed for autoimmune diseases and organ transplantation (*4*). Rapid advances in genome engineering have raised hopes that conventional T cells and Tregs can be reprogrammed using precise genome targeting.

A variety of approaches have been used to modify the genomes of primary human T cells. Long DNA sequences (multiple kilobases) can be inserted using lentiviral vectors, but the integration sites are non-targeted (*5*). Lentiviruses have been the primary means to introduce gene constructs such as chimeric antigen receptors (CARs) (*6*). To knock out specific endogenous genes, sequence specific nucleases such as Cas9, TALEN or zinc-finger nuclease (ZFN) can be electroporated into T cells (*7*, *8*), generating double-stranded breaks that result in a non-random spectrum of insertions and deletion mutations through non-homologous end-joining (NHEJ) (*9*). Co-delivery of small (<200 bp) chemically synthesized ssDNA oligos (ssODNs) that have homology to the sequences flanking a specific nuclease cleavage site has been used to modify short DNA sequences via homology directed repair (*7*).

The targeted integration of much longer DNA sequences would enable more diverse applications. This has recently been achieved by electroporation of a sequence-specific nuclease followed by infection with an integrase-deficient adeno-associated vector (AAV) containing an HDR template (*10*, *11*). This electroporation and infection approach has enabled novel therapeutic T cell engineering strategies (*12*) but causes off-target integrations, necessitates a potentially undesirable viral infection, and is limited in throughput due to challenges in viral production.

We systematically tested cell culture conditions, concentrations of Cas9 RNPs and HDR templates and electroporation parameters to develop an optimized method for high-efficiency non-viral genome targeting. We identified conditions where high concentrations of Cas9 RNPs and long DNA templates (>1 Kb) could be co-delivered into multiple loci in primary human T cells with limited effects on cell viability.

Non-viral targeting could be used to correct a pathogenic mutation that causes Treg dysfunction and monogenic autoimmune disease. We describe a family where two children have developed early onset autoimmune disease and a third has autoantibodies suggesting a very high risk of type 1 diabetes (T1D) and identified the causal loss-of-function mutations in *IL2RA* through exome sequencing. IL2RA is critical for regulatory T cell function and immune homeostasis. With our optimized non-viral CRISPR genome targeting, we achieved efficient mutation correction, which restored cell surface expression of IL2RA along with functional downstream signaling. Non-viral genome targeting in primary human immune cells will enable functional studies and correction of mutations in cells from patients. Cell therapies coupled with improved gene targeting (non-viral templates, high efficiency and specificity, and long targeting constructs) hold enormous promise for treatment of autoimmune diseases as well as immune deficiencies, infectious diseases, organ transplantation and cancer immunotherapy.

Development of non-viral human T cell genome targeting

A major limitation for genome targeting in human T cells has been that DNA delivery leads to cell death (*13*). While the introduction of short single-stranded oligodeoxynucleotide (ssODN) HDR templates did not cause significant loss of viability in T cells, larger linear dsDNA templates led to extensive toxicity (*14*, *15*). We found that long (>1kb) linear dsDNA templates were less toxic when they were co-electroporated with a CRISPR-Cas9 ribonucleoprotein (Cas9 RNP) (fig. S1). This suggested that co-delivery of an appropriate mixture of Cas9 RNPs and long dsDNA would enable HDR and preserve cell viability.

We systematically optimized non-viral genome targeting in primary human T cells. The protocol was adjusted for efficiency of target integration, cell viability, and the total number of integration-positive cells (**Fig. 1A** and fig. S2). Cas9 RNPs were electroporated along with a dsDNA HDR template designed to introduce an N-terminal GFP-fusion to the housekeeping gene *RAB11A* (**Fig. 1B**). High-throughput flow cytometry performed 3-5 days after electroporation was used to monitor integration and cell viability. First, we identified stimulation and cytokine treatments both before and after electroporation that markedly increased rates of gene targeting (**Fig. 1C** and fig. S3 and S4). These conditions allowed efficient targeting in fresh or frozen primary T cells isolated from a variety of sources (fig. S5). Varying ratios of Cas9 RNP and HDR template concentrations were tested at different amounts in these well-stimulated T cells, (**Fig. 1D** and fig. S6), and appropriate concentrations were identified that enabled efficient gene targeting. Finally, we tested electroporation conditions to maximize gene targeting while preserving high levels of cell viability (**Fig. 1E** and fig. S7). Non-viral gene targeting could achieve introduction of a GFP fusion to the endogenous *RAB11A* housekeeping gene in over 50% of cells in both primary human CD4+ and CD8+ T cells (**Fig. 1F**).

Rapid and combinatorial gene targeting applications

The simplicity and speed of non-viral gene targeting allowed us to apply it across genomic sites and human blood donors (**Fig. 2** and fig. S2). Constructs encoding GFP-fusions with homologous flanking sequences were efficiently and reproducibly targeted to a variety of sites throughout the genome (**Fig. 2A** and fig. S8). These targeted GFP fusions labeled a variety of sub-cellular structures (*17*). Confocal microscopy confirmed the specificity of the fusion proteins produced by targeting diverse genes, and also demonstrated that targeting endogenous genes with GFP enabled imaging of protein localization in living human T cells (**Fig. 2B**). In cells from a cohort of a dozen healthy human donors, targeting GFP integrations into diverse genes proved highly reproducible in primary human T cells (fig. S8 and S9). The specificity of the targeted integrations and the cell-type specific expression pattern of the tagged genes was confirmed further by tagging the endogenously-encoded CD4 surface receptor with GFP. We observed a linear relationship between CD4 and GFP expression specifically in tagged CD4+ T cells but not in CD8+ T cells (**Fig. 2C**). Taken together, these findings establish that non-viral genome targeting can be used to modify endogenous genes by inserting large DNA sequences into targeted sites in the genome.

Fusion tags not only permitted imaging of endogenous proteins, but also could be used for biochemical targeting of specific proteins. For example, ChIP-Seq, and more recently CUT & RUN (*18*), are widely used to map transcription factor binding sites; however these assays are often limited by availability of effective and specific antibodies. As a proof-of-principle we used

anti-GFP antibodies to perform CUT & RUN in primary T cells where the endogenous gene encoding BATF, a critical TF, had been targeted to generate a GFP-fusion. Binding sites identified with anti-GFP CUT & RUN closely matched the sites identified with anti-BATF antibody (**Fig. 2D** and fig. S10).

Targeting two alleles of the same gene with two distinct fluorophores would provide a way to quantify and enrich cells with bi-allelic gene modifications. We introduced two distinct fluorescent proteins targeting the same site at the *RAB11A* gene (**Fig. 3A** and fig. S11) and showed that >5% of cells had successful bi-allelic integrations. Importantly, the number of cells that express both fluorescent proteins underestimates the percentage of cells with bi-allelic integrations because some cells will have received either GFP or mCherry on both alleles. We constructed a model to account for homozygous integrations of the same fluorescent protein (**Fig. 3B**, fig. S11 and supplementary text). This model estimates that there were bi-allelic integrations in the *RAB11A* gene in up to ~10% of cells. This suggests that cells with one *RAB11A* integration are more likely to have also undergone a second targeted integration, and this effect was observed across three genomic loci (fig. S11). Co-delivery of three fluorescent-tags targeting the *RAB11A* locus demonstrated very low rates of cells that express all three fluorophores, consistent with low rates of off-target integrations in these experiments (fig. S11G). In summary, using multiple non-viral constructs to targeting the same locus allows identification of bi-allelic genome editing in human T cells.

Multiplex editing of combinatorial sets of genomic sites would offer expanded research and therapeutic applications. We tested whether multiple non-viral HDR templates could be co-delivered with multiple RNPs to generate primary cells with more than one modified locus. We found not only that multiplexed gene targeting was possible (**Fig. 3C**), but that cells with two modifications were enriched by gating on the cells that had one modification (**Fig. 3D and fig. S12**) (*19*). We were also able to achieve triple gene targeting and could significantly enrich for cells that had a third modification by gating on the cells with two targeted insertions (**Fig. 3E and fig. S12**). Overall, non-viral gene targeting can be used to enable complex genetic modifications of primary T cells that could be used for a variety of research and therapeutic applications.

D10A nickase and ssDNA HDR templates reduce off-target integrations

One of the major concerns using HDR templates, especially for therapeutic applications, is the potential for off-target integrations. This has been observed even when integrase-deficient AAVs were used as donor templates (*20*). We similarly found evidence of functional off-target integrations using a linear dsDNA template for non-viral gene targeting. Double-stranded DNA templates can integrate in an HDR-independent manner at sites of naturally occurring dsDNA breaks (*21*), as well as at the specific dsDNA breaks induced by targeted nucleases such as Cas9 — an effect called Homology-Independent Targeted Integration (*22*, *23*). We looked for unintended non-homologous integrations using an N-terminal GFP-RAB11A fusion construct which contained the endogenous *RAB11A* promoter sequence within its 5' homology arm; this construct can drive GFP expression at off-target integration sites (**Fig. 4A** and fig. S13). We found that functional off-target integrations were present in cells from different biological donors (**Fig. 4B**), and were seen in experiments with different target sequences and HDR templates (fig. S13 and S14). Off-target integrations must be minimized in cells destined for therapeutic use to

ensure that integrated sequences remain under proper endogenous regulation and that off-target sites are not disrupted.

To reduce off-target integrations caused by off-target Cas9 cutting, we performed non-viral gene targeting using the D10A Cas9 nickase variant. This variant requires that two gRNAs bind and cleave in close proximity to produce a double strand break, thus reducing the number of off-target dsDNA breaks (*24–26*). We tested a series of gRNA combinations at the *RAB11A* locus for GFP integration, and found a set of "PAM-Out" guides that showed efficient introduction of GFP when using the D10A nickase (fig. S15). As expected, use of D10A with a single off-target guide showed markedly reduced functional off-target integrations when compared to Cas9, equivalent to the level seen when nuclease-incompetent dCas9 was used (**Fig. 4C**).

Even using the D10A nickase, dsDNA HDR templates still gave rise to rare but observable off-target integrations (comparable to the rate observed with no Cas9 nuclease), perhaps at naturally occurring dsDNA breaks (**Fig. 4A and C**). We reasoned that the remaining off-target integrations could be eliminated by replacing the dsDNA HDR templates with long ssDNA HDR templates, which cannot integrate non-specifically at double strand breaks (*27, 28*). To test this hypothesis, we generated ssDNA HDR templates with two methods we recently developed that produce the large amounts of long ssDNA required for electroporation (fig. S16) (*28*) ssDNA HDR templates reduced functional off-target integrations approximately 100-fold, while maintaining efficient on-target integration (**Fig. 4D** and fig. S16). We were able to use D10A Cas9 nickase with ssDNA templates. In these experiments, although on-target integration rates were reduced, non-specific integrations were reduced to background levels seen without template (**Fig. 4E and F**). For sites where potential off-target activity is a concern, D10A Cas9 nickase and ssDNA HDR templates can be employed to reduce the rates of integration arising from off-target induced double strand breaks and naturally occurring breaks respectively, which may make this an attractive method for therapeutic modification of patient T cells.

Therapeutic mutation correction by non-viral gene targeting

We sought to apply non-viral gene targeting to correct the mutations that cause monogenic immune dysregulation in T cells from patients. We identified a family with monogenic primary immune dysregulation with autoimmune disease caused by recessive loss-of-function mutations in the gene encoding the IL-2 alpha receptor (IL2RA), also known as CD25 (*29–31*). IL2RA is essential for Tregs and immune homeostasis (*32*, *33*), and the children in the family who are compound heterozygotes with two loss-of-function mutations have pleiotropic autoimmune manifestations (Table 1). One is affected by neonatal-onset type 1 diabetes (T1D) and another has developed recalcitrant autoimmune cytopenias during childhood. All three IL2RA-deficient family members demonstrated pathologic serum autoantibodies. The IL2RA-deficient children have an almost complete loss of IL2RA cell surface expression and therefore virtually no detectable $CD3^{+}CD4^{+}CD25^{hi}CD127^{lo}$ Tregs in their blood, whereas family relatives carrying heterozygous *IL2RA* mutations display decreased IL2RA expression on their Tregs (fig. S17). However, frequencies of $CD3^{+}CD4^{+}CD127^{lo}FOXP3^{+}$ T cells in the IL2RA-deficient subjects resemble those in healthy donors (HD) and heterozygous family members, suggesting that Treg-like cells develop and persist despite the IL2RA mutations. Using a strategy to isolate Tregs without CD25 expression, we found that $CD3^{+}CD4^{+}CD127^{lo}CD45RO^{+}TIGIT^{+}$ Treg-

enriched cells from CD25-deficient subjects showed a defective ability to suppress the proliferation of responder T cells (Tresps) as compared to HD counterparts (fig. S17). In contrast, Tregs from relatives with a single heterozygous *IL2RA* mutation could inhibit Tresp proliferation, albeit with suboptimum capacity (fig. S17). Hence, correcting functional IL2RA expression on the surface of $FOXP3^+$ T cells from these patients may represent a valuable approach for developing an *ex vivo* gene therapy.

Whole exome sequencing revealed that the IL2RA deficient children harbored compound heterozygous mutations in *IL2RA* (**Fig. 5A** and fig. S18). One mutation at c.530A>G creates a premature stop codon. Improvements in cell culture and electroporation methodologies made it possible to efficiently correct the mutation using ~120 bp chemically synthesized ssDNA HDR templates (fig. S19). Rates were even higher using a longer dsDNA template (**Fig. 5B** and fig. S19 and S20). The corrected patient-derived T cells expressed IL2RA on their surface. Although correction was successful in all three siblings, lower rates of IL2RA expression were seen in compound het 3, which could be due to altered cell-state associated with the patient's disease or the fact she was on the only sibling treated with immunosuppression (Table 1 and fig. S21). The second mutation, c.800delA, causes a frameshift in the reading frame of the final IL2RA exon resulting in misreading of the portion of the gene encoded in the final exon as well as run-on translation past the normal stop codon. This frameshift could be ameliorated even without an HDR template (fig. S20). At this site, genomic cutting caused by a Cas9 RNP alone was sufficient to cause productive cell surface expression of IL2RA, likely by restoring the correct frame with insertion/deletion mutations (fig. S20). Taken together, these data show how distinct mutations can be corrected in patient T cells with HDR template-dependent and non-HDR template-dependent repair mechanisms.

One potential therapeutic strategy for patients from this family with monogenic Treg defects would be *ex vivo* T cell gene correction followed by transfusion of autologous corrected Tregs. Treg cells produced by targeted correction could limit some of the potential risks of hematopoietic stem cell transplantation. We tested whether correcting one of the IL2RA mutations led to productive signaling and whether or not correction occurred in a meaningful fraction of FOXP3+ Tregs. Following correction of the c.530A>G mutation, cells were able to functionally signal through IL2RA, the high-affinity IL-2 receptor. In response to IL-2 treatment, the modified cells demonstrated increased STAT5 phosphorylation, a hallmark of productive signaling (**Fig. 5C** and fig. S19 and S20). In addition, flow cytometry confirmed that a fraction of IL2RA corrected cells expressed FOXP3, a critical transcriptional factor in Tregs (**Fig. 5D** and fig. S19 and S20).

The endogenous gene encoding IL2RA is under tight control by multiple cis-regulatory elements that constitute a super-enhancer (*34, 35*). Therefore, therapeutic correction of IL2RA is likely to depend on specific repair of the gene in its endogenous genomic locus. Given that GFP insertions with Cas9 and dsDNA showed that there is a potential for non-specific integrations of dsDNA, we used D10A Cas9 nickase and a long ssDNA template to specifically repair the c.530A>G patient mutation. Using these reagents we were able to specifically and selectively correct the mutant gene in ~20% of the T cells from the patient (**Fig. 5E**).

Discussion

Non-viral gene targeting enables efficient insertion of defined sequences throughout the genome of primary human T cells. These insertions can range from the introduction or correction of single base pair mutations, to integration of large functional sequences and tags at endogenous loci, and multiplexed integrations throughout the genome are possible. For therapeutic applications of engineered T cells, off-target integrations can be significantly reduced by using D10A Cas9 nickase and a ssDNA HDR template. Our findings will enable the accelerated development of engineered T cell therapies and the treatment of genetic disease.

References and Notes:

1. A. D. Fesnak, C. H. June, B. L. Levine, Engineered T cells: the promise and challenges of cancer immunotherapy. *Nat. Rev. Cancer*. **16**, 566–581 (2016).
2. J. H. Esensten, J. A. Bluestone, W. A. Lim, Engineering Therapeutic T Cells: From Synthetic Biology to Clinical Trials. *Annu. Rev. Pathol.* **12**, 305–330 (2017).
3. K. T. Roybal, W. A. Lim, Synthetic Immunology: Hacking Immune Cells to Expand Their Therapeutic Capabilities. *Annu. Rev. Immunol.* **35**, 229–253 (2017).
4. J. A. Bluestone *et al.*, Type 1 diabetes immunotherapy using polyclonal regulatory T cells. *Sci. Transl. Med.* **7**, 315ra189 (2015).
5. E. Verhoeyen, C. Costa, F.-L. Cosset, in *Methods in Molecular Biology* (2009), pp. 97–114.
6. M. Kalos *et al.*, T cells with chimeric antigen receptors have potent antitumor effects and can establish memory in patients with advanced leukemia. *Sci. Transl. Med.* **3**, 95ra73 (2011).
7. K. Schumann *et al.*, Generation of knock-in primary human T cells using Cas9 ribonucleoproteins. *Proceedings of the National Academy of Sciences*. **112**, 10437–10442 (2015).
8. E. E. Perez *et al.*, Establishment of HIV-1 resistance in CD4+ T cells by genome editing using zinc-finger nucleases. *Nat. Biotechnol.* **26**, 808–816 (2008).
9. M. van Overbeek *et al.*, DNA Repair Profiling Reveals Nonrandom Outcomes at Cas9-Mediated Breaks. *Mol. Cell*. **63**, 633–646 (2016).
10. B. D. Sather *et al.*, Efficient modification of CCR5 in primary human hematopoietic cells using a megaTAL nuclease and AAV donor template. *Sci. Transl. Med.* **7**, 307ra156 (2015).
11. N. Hubbard *et al.*, Targeted gene editing restores regulated CD40L function in X-linked hyper-IgM syndrome. *Blood*. **127**, 2513–2522 (2016).
12. J. Eyquem *et al.*, Targeting a CAR to the TRAC locus with CRISPR/Cas9 enhances tumour rejection. *Nature*. **543**, 113–117 (2017).
13. T. I. Cornu, C. Mussolino, T. Cathomen, Refining strategies to translate genome editing to the clinic. *Nat. Med.* **23**, 415–423 (2017).
14. Y. Zhao *et al.*, High-Efficiency Transfection of Primary Human and Mouse T Lymphocytes Using RNA Electroporation. *Mol. Ther.* **13**, 151–159 (2006).
15. V. Hornung, E. Latz, Intracellular DNA recognition. *Nat. Rev. Immunol.* **10**, 123–130 (2010).
16. J. F. Hultquist *et al.*, A Cas9 Ribonucleoprotein Platform for Functional Genetic Studies of HIV-Host Interactions in Primary Human T Cells. *Cell Rep.* **17**, 1438–1452 (2016).
17. M. D. Leonetti, S. Sekine, D. Kamiyama, J. S. Weissman, B. Huang, A scalable strategy for high-throughput GFP tagging of endogenous human proteins. *Proc. Natl. Acad. Sci. U. S. A.* **113**, E3501–8 (2016).

18. P. J. Skene, S. Henikoff, An efficient targeted nuclease strategy for high-resolution mapping of DNA binding sites. *Elife*. **6** (2017), doi:10.7554/eLife.21856.

19. D. Agudelo *et al.*, Marker-free coselection for CRISPR-driven genome editing in human cells. *Nat. Methods*. **14**, 615–620 (2017).

20. D. P. Dever *et al.*, CRISPR/Cas9 β-globin gene targeting in human haematopoietic stem cells. *Nature*. **539**, 384–389 (2016).

21. J. P. Murnane, M. J. Yezzi, B. R. Young, Recombination events during integration of transfected DNA into normal human cells. *Nucleic Acids Res.* **18**, 2733–2738 (1990).

22. T. O. Auer, K. Duroure, A. De Cian, J.-P. Concordet, F. Del Bene, Highly efficient CRISPR/Cas9-mediated knock-in in zebrafish by homology-independent DNA repair. *Genome Res.* **24**, 142–153 (2014).

23. K. Suzuki *et al.*, In vivo genome editing via CRISPR/Cas9 mediated homology-independent targeted integration. *Nature*. **540**, 144–149 (2016).

24. Y. Miyaoka *et al.*, Systematic quantification of HDR and NHEJ reveals effects of locus, nuclease, and cell type on genome-editing. *Sci. Rep.* **6** (2016), doi:10.1038/srep23549.

25. L. E. M. Vriend *et al.*, Distinct genetic control of homologous recombination repair of Cas9-induced double-strand breaks, nicks and paired nicks. *Nucleic Acids Res.* **44**, 5204–5217 (2016).

26. A. Bothmer *et al.*, Characterization of the interplay between DNA repair and CRISPR/Cas9-induced DNA lesions at an endogenous locus. *Nat. Commun.* **8**, 13905 (2017).

27. R. M. Quadros *et al.*, Easi-CRISPR: a robust method for one-step generation of mice carrying conditional and insertion alleles using long ssDNA donors and CRISPR ribonucleoproteins. *Genome Biol.* **18**, 92 (2017).

28. Leonetti *et al.* http://www.biorxiv.org/content/early/2017/08/21/178905

29. N. Sharfe, H. K. Dadi, M. Shahar, C. M. Roifman, Human immune disorder arising from mutation of the alpha chain of the interleukin-2 receptor. *Proc. Natl. Acad. Sci. U. S. A.* **94**, 3168–3171 (1997).

30. A. A. Caudy, S. T. Reddy, T. Chatila, J. P. Atkinson, J. W. Verbsky, CD25 deficiency causes an immune dysregulation, polyendocrinopathy, enteropathy, X-linked–like syndrome, and defective IL-10 expression from CD4 lymphocytes. *J. Allergy Clin. Immunol.* **119**, 482–487 (2007).

31. K. Goudy *et al.*, Human IL2RA null mutation mediates immunodeficiency with lymphoproliferation and autoimmunity. *Clin. Immunol.* **146**, 248–261 (2013).

32. S. Sakaguchi, N. Sakaguchi, M. Asano, M. Itoh, M. Toda, Immunologic self-tolerance maintained by activated T cells expressing IL-2 receptor alpha-chains (CD25). Breakdown of a single mechanism of self-tolerance causes various autoimmune diseases. *J. Immunol.* **155**, 1151–1164 (1995).

33. A. Y. Rudensky, Regulatory T cells and Foxp3. *Immunol. Rev.* **241**, 260–268 (2011).

34. K. K.-H. Farh *et al.*, Genetic and epigenetic fine mapping of causal autoimmune disease variants. *Nature*. **518**, 337–343 (2015).

35. Simeonov et al Discovery of Stimulation-Responsive Immune Enhancers with Unbiased CRISPR Activation. *Nature.* In press.

Acknowledgments: We thank members of the Marson lab, Chris Jeans and the QB3 MacroLab, Kyle Marchuk and the UCSF Biological Imaging Development Center, and Jacob Corn for suggestions and technical assistance. We thank Lonza for technical assistance and providing reagents to test electroporation conditions. This research was supported by NIH grants DP3DK111914-01 and P50GM082250 (A.M.), a grant from the Keck Foundation (A.M.), gifts from Jake Aronov and Galen Hoskin (A.M.), a gift from the Jeffrey Modell Foundation, and a National Multiple Sclerosis Society grant (A.M.; CA 1074-A-21). T.L.R. and J.H. were supported by the UCSF Medical Scientist Training Program (T32GM007618). T.L.R. was supported by the UCSF Endocrinology Training Grant (T32 DK007418). A.M. holds a Career Award for Medical Scientists from the Burroughs Wellcome Fund and is a Chan Zuckerberg Biohub Investigator. We also relied on the Flow Cytometry Core at UCSF, supported by the Diabetes Research Center grant NIH P30 DK063720. A.M. is co-founder of Spotlight Therapeutics. A.M. serves as an advisor to Juno Therapeutics and PACT Therapeutics and the Marson lab has received sponsored research support from Juno Therapeutics and Epinomics. A provisional patent was filed based on results described here.

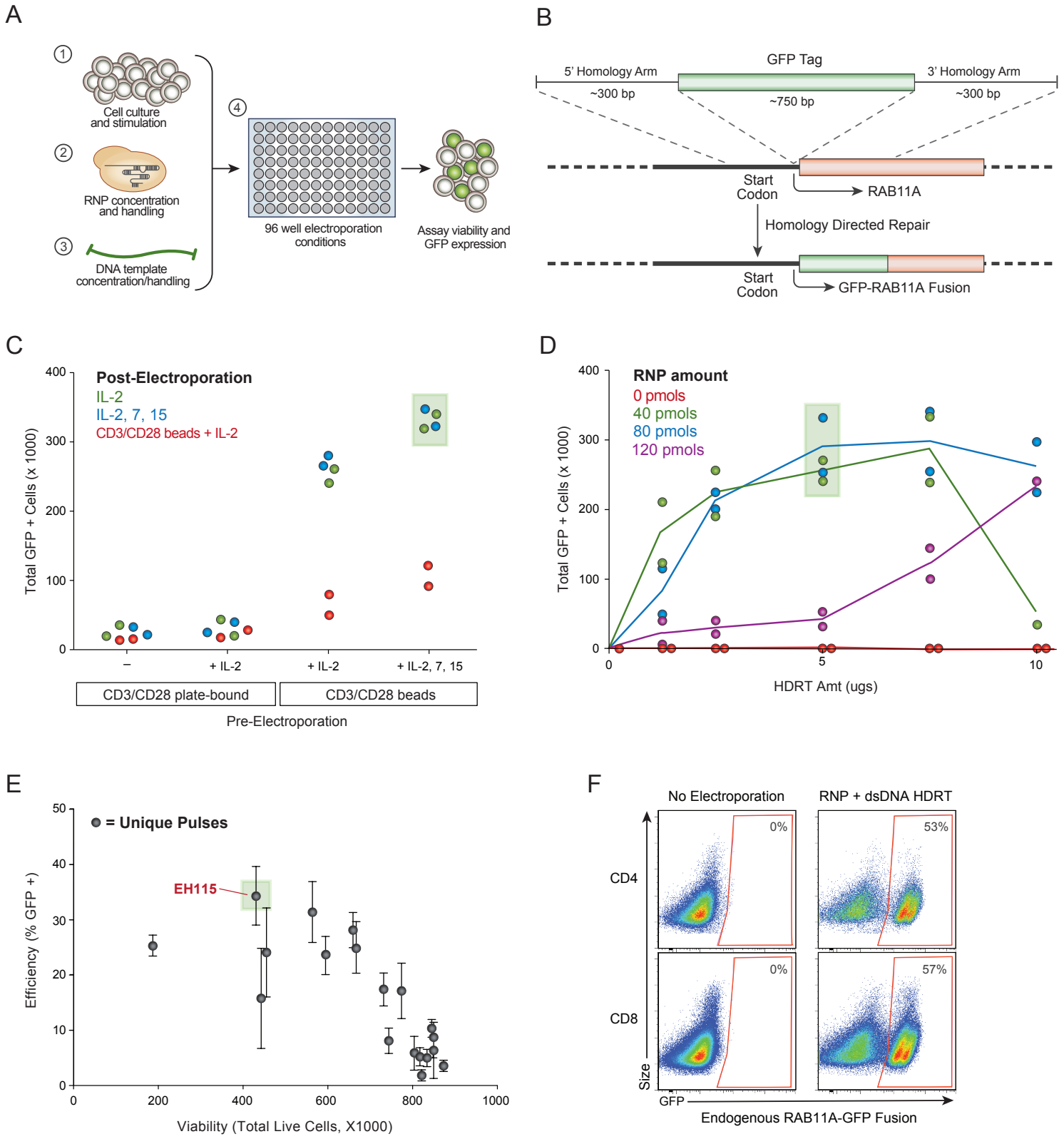
A
1
Cell culture and stimulation
2
RNP concentration and handling
3
DNA template concentration/handling
4
96 well electroporation conditions
Assay viability and GFP expression
B
GFP Tag
5' Homology Arm
3' Homology Arm
~300 bp
~750 bp
~300 bp
Start Codon
RAB11A
Homology Directed Repair
Start Codon
GFP-RAB11A Fusion
C
Post-Electroporation
IL-2
IL-2, 7, 15
CD3/CD28 beads + IL-2
Total GFP + Cells (x 1000)
400
300
200
100
0
–
+ IL-2
+ IL-2
+ IL-2, 7, 15
CD3/CD28 plate-bound
CD3/CD28 beads
Pre-Electroporation
D
RNP amount
0 pmols
40 pmols
80 pmols
120 pmols
Total GFP + Cells (x 1000)
400
300
200
100
0
0
5
10
HDRT Amt (ugs)
E
= Unique Pulses
EH115
Efficiency (% GFP +)
50
40
30
20
10
0
0
200
400
600
800
1000
Viability (Total Live Cells, X1000)
F
No Electroporation
RNP + dsDNA HDRT
CD4
CD8
0%
53%
0%
57%
Size
GFP
Endogenous RAB11A-GFP Fusion

Fig. 1. Development of efficient large non-viral gene targeting.
(A) Systematic analysis of the effects of cell culture and stimulation conditions, RNP and DNA template formulations, and electroporation conditions via 96-well high-throughput electroporations enabled rapid optimization of both cell viability (total number of live cells in culture) and HDR efficiency (% of cells GFP positive). **(B)** Schematic of a long (1350bp) linear dsDNA template encoding a GFP sequence flanked by regions homologous to the N-terminus of the housekeeping gene *RAB11A* (not drawn to scale). When a dsDNA break is induced at the N-terminus of *RAB11A*, the GFP sequence can be seamlessly introduced via homology directed repair (HDR) to generate an endogenously-tagged RAB11A-GFP fusion protein. **(C)** Primary human T cells were cultured for 2 days using varying combinations of T cell receptor (TCR) stimulation and cytokines prior to electroporation of *RAB11A* targeting RNP and HDR template, followed by varying culture conditions for 5 days post-electroporation. **(D)** Among RNP and HDR template concentrations tested here, optimal GFP insertion into *RAB11A* was achieved at intermediate concentrations of the reagents. Further testing (fig. S6) narrowed optimal concentrations to 50 pmols of RNP and 4 ugs of dsDNA HDRT. **(E)** Arrayed testing of electroporation pulse conditions showed that, in general, conditions yielding higher HDR efficiency decreased viability. EH115 was selected to optimize HDR, while still maintaining sufficient viability. **(F)** Using parameters optimized in **C-D**, high-efficiency insertion of GFP into the endogenous *RAB11A* gene was achieved by non-viral targeting in both primary human $CD4^+$ and $CD8^+$ T cells. Viability and efficiency were assayed 3 days (**E**) or 5 days (**C**, **D**, and **F**) after electroporation. Individual points represent individual blood donors (**C** and **D**) or the mean plus standard deviation in two individual donors (E). Green highlights indicate conditions ultimately chosen for the non-viral gene targeting protocol.

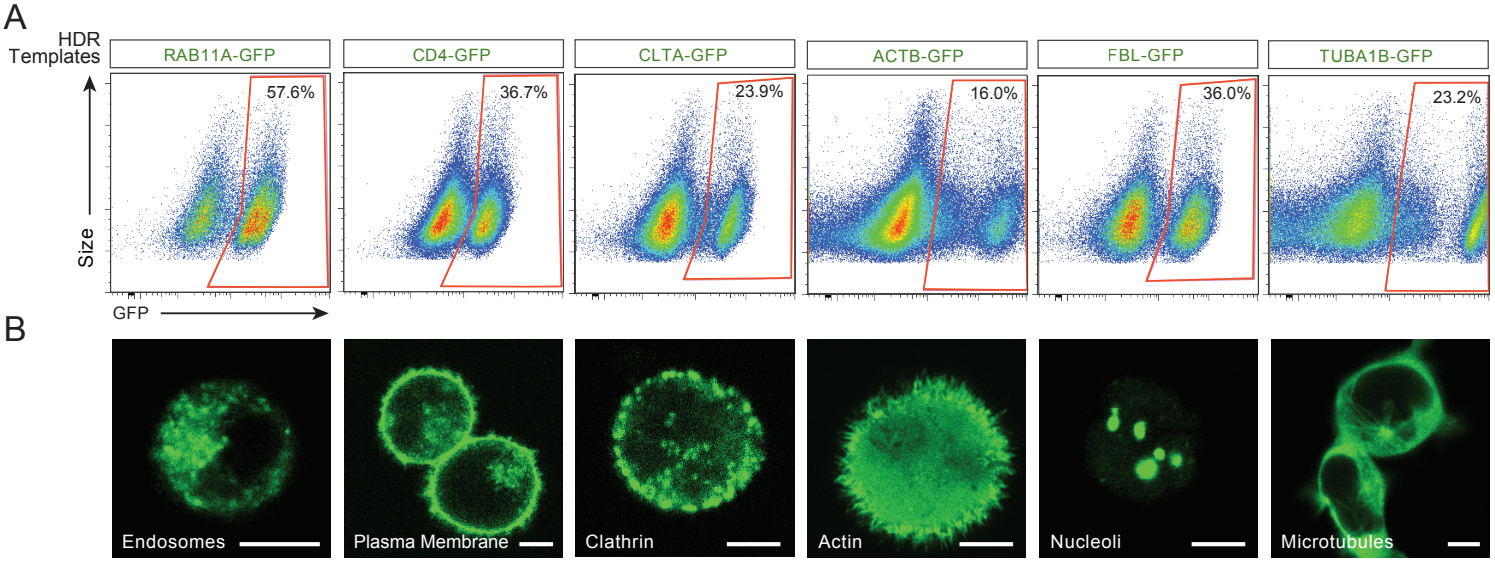
A
HDR Templates
RAB11A-GFP
CD4-GFP
CLTA-GFP
ACTB-GFP
FBL-GFP
TUBA1B-GFP
57.6%
36.7%
23.9%
16.0%
36.0%
23.2%
Size
GFP
B
Endosomes
Plasma Membrane
Clathrin
Actin
Nucleoli
Microtubules

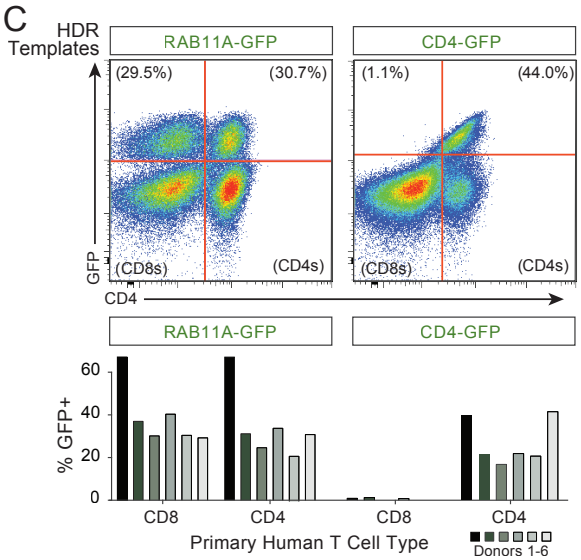
C
HDR Templates
RAB11A-GFP
CD4-GFP
(29.5%)
(30.7%)
(1.1%)
(44.0%)
(CD8s)
(CD4s)
(CD8s)
(CD4s)
GFP
CD4
RAB11A-GFP
CD4-GFP
% GFP+
60
40
20
0
CD8
CD4
CD8
CD4
Primary Human T Cell Type
Donors 1-6

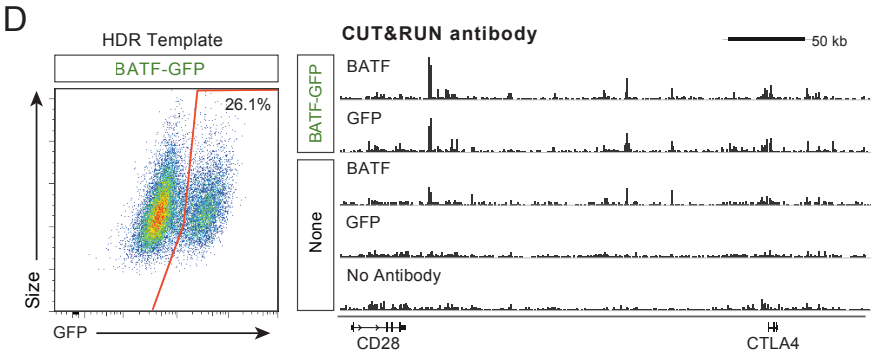
D
HDR Template
BATF-GFP
26.1%
Size
GFP
CUT&RUN antibody
50 kb
BATF-GFP
BATF
GFP
None
BATF
GFP
No Antibody
CD28
CTLA4

Fig. 2. Diverse applications of non-viral gene targeting in primary human T cells.
(A) High efficiency genome targeting with GFP-fusion constructs could be achieved in multiple endogenous genes in primary human T cells using non-viral HDR templates and corresponding RNPs. **(B)** Confocal microscopy of living, primary human T cells 7 days after electroporation of the indicated HDR template confirmed the specificity of fusion-protein targeting. Scale bar in each image is 5 um. **(C)** Non-viral targeting of GFP-fusion constructs to the *RAB11A* and *CD4* genes in bulk human primary T cells. RAB11A-fusions were GFP positive in both CD4+ and CD8+ cells, whereas CD4+-fusions were only positive in CD4+ T cells (representative flow cytometry above, quantification below). **(D)** Primary human T cells were engineered to express GFP fused to the endogenous transcription factor, BATF. At 11 Days post electroporation, nuclei were isolated and CUT&RUN was performed. GFP-BATF and total BATF chromatin interaction sites were identified using anti-GFP or anti-BATF antibodies. Flow cytometry to assay viability and efficiency was performed at 4 days after electroporation (**A**, **C**, **D**). Displayed data is representative of at least two different donors.

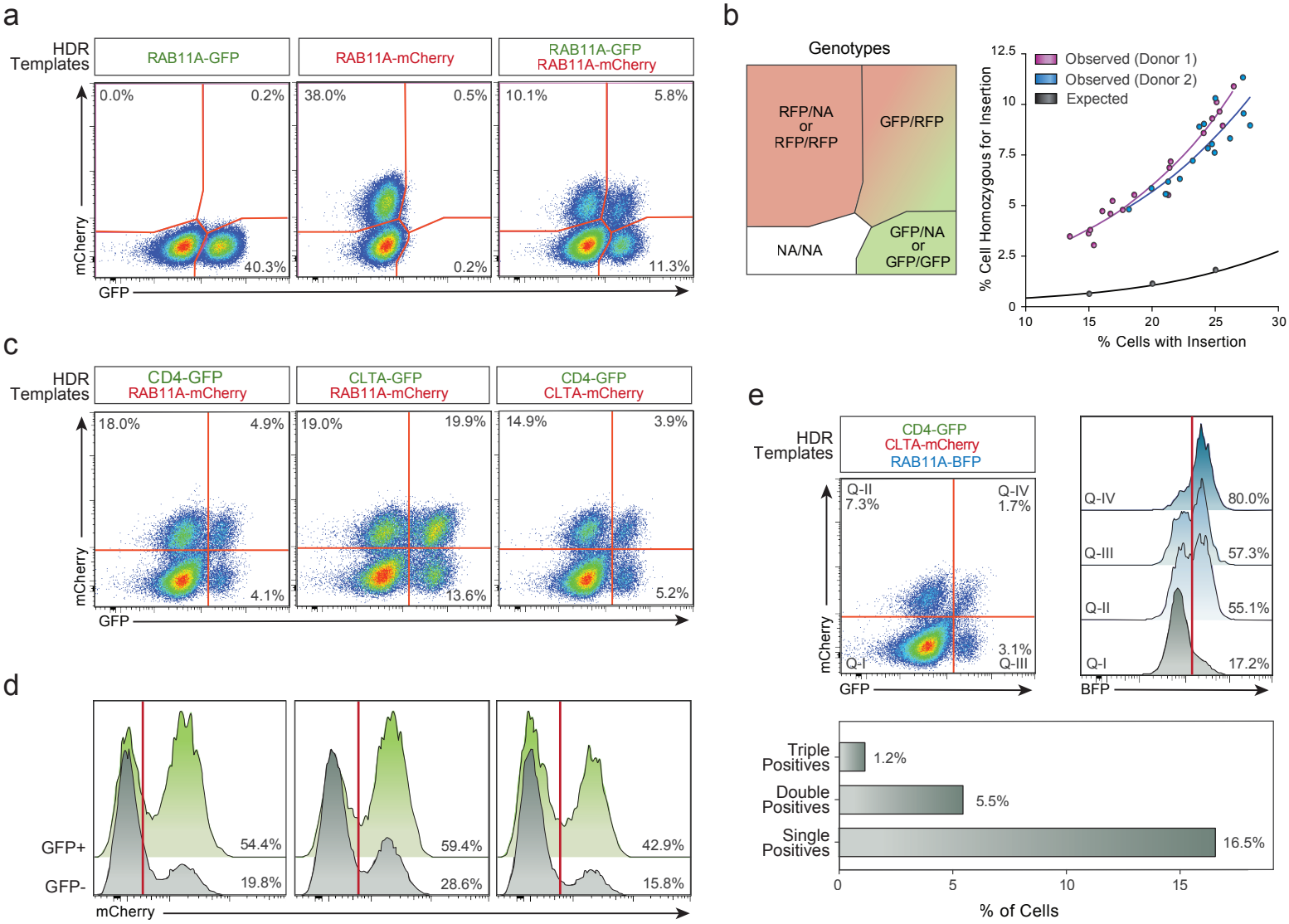
a
HDR Templates
RAB11A-GFP
RAB11A-mCherry
RAB11A-GFP
RAB11A-mCherry
0.0%
0.2%
40.3%
38.0%
0.5%
0.2%
10.1%
5.8%
11.3%
mCherry
GFP
b
Genotypes
RFP/NA or RFP/RFP
GFP/RFP
NA/NA
GFP/NA or GFP/GFP
Observed (Donor 1)
Observed (Donor 2)
Expected
% Cell Homozygous for Insertion
% Cells with Insertion
c
HDR Templates
CD4-GFP
RAB11A-mCherry
CLTA-GFP
RAB11A-mCherry
CD4-GFP
CLTA-mCherry
18.0%
4.9%
4.1%
19.0%
19.9%
13.6%
14.9%
3.9%
5.2%
mCherry
GFP
d
GFP+
GFP-
54.4%
19.8%
59.4%
28.6%
42.9%
15.8%
mCherry
e
HDR Templates
CD4-GFP
CLTA-mCherry
RAB11A-BFP
Q-II
7.3%
Q-IV
1.7%
Q-I
3.1%
Q-III
mCherry
GFP
Q-IV
80.0%
Q-III
57.3%
Q-II
55.1%
Q-I
17.2%
BFP
Triple Positives
1.2%
Double Positives
5.5%
Single Positives
16.5%
% of Cells

Fig. 3. Combinatorial non-viral gene targeting.
(A) Simultaneous electroporation of HDR templates to create RAB11A-GFP and/or RAB11A-mCherry fusions in primary human T cells. A distinct population of dual GFP+ mCherry+ cells was found when both templates are introduced concurrently, consistent with bi-allelic targeting. **(B)** The potential genotypes for individual cells in the quadrants are defined by expression of the two fluorophores. The observed level of bi-allelic integrations is higher in cells that acquire at least one integration than expected by chance (fig. S11). Individual points represent replicates where the combination of the genes encoding the fluorescent proteins was varied (GFP + mCherry, GFP + BFP, mCherry + BFP) as was the amount of HDR template (3 to 6 ugs). **(C-D)** Multiplexed integration of HDR Templates at two separate genomic loci in the same primary human T cells. 2 ugs of each template (4 ugs total per electroporation) were electroporated together with 25 pmols of each RNP (50 pmols total). Cells positive for integration at one site (e.g. GFP+) were much more likely to have an integration at the second site (e.g. also be mCherry+) than cells lacking the first integration. **(E)** Simultaneous non-viral gene targeting of large insertions to three distinct genomic loci. 1.5 ugs of each template (4.5 ugs total) were electroporated together with 20 pmols of each corresponding RNP (60 pmols total). Similarly to two site multiplexing, cells positive for a single integration (mCherry+ in Q-II and GFP+ in Q-III) were more likely to have a second integration (BFP+) compared to those without (Q-I). Cells positive for two integrations (GFP+ and mCherry+, Q-IV) are even more likely to have an integration of the third gene (BFP+). Below is a bar graph quantification of cells that are single, double and triple positive for fluorophores. All fluorescent readouts were performed 4 days post-electroporation. Displayed data are representative of at least two different donors except panel E (one donor).

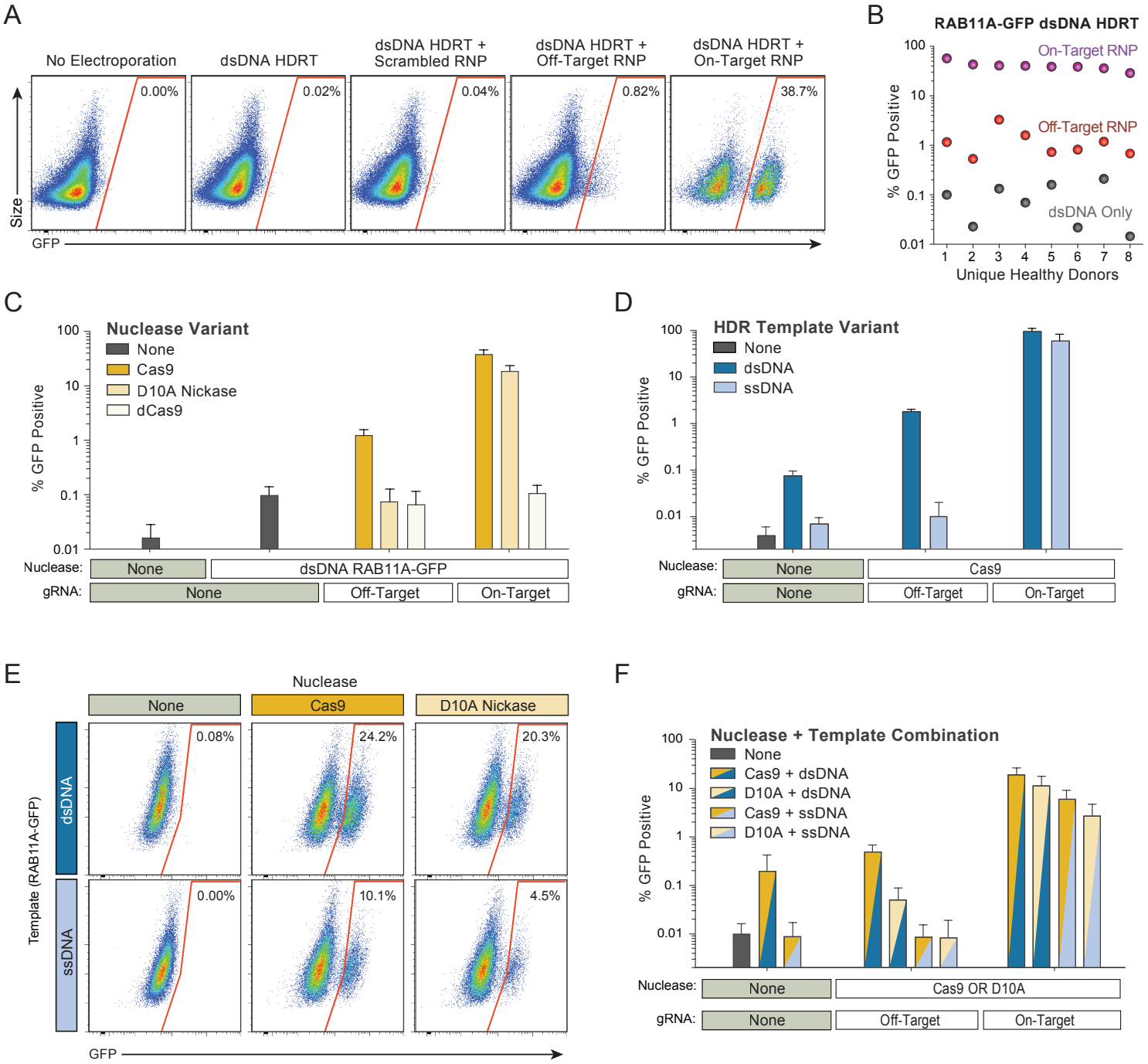
A
No Electroporation
dsDNA HDRT
dsDNA HDRT + Scrambled RNP
dsDNA HDRT + Off-Target RNP
dsDNA HDRT + On-Target RNP
0.00%
0.02%
0.04%
0.82%
38.7%
Size
GFP
B
RAB11A-GFP dsDNA HDRT
On-Target RNP
Off-Target RNP
dsDNA Only
% GFP Positive
Unique Healthy Donors
C
Nuclease Variant
None
Cas9
D10A Nickase
dCas9
% GFP Positive
Nuclease:
None
dsDNA RAB11A-GFP
gRNA:
None
Off-Target
On-Target
D
HDR Template Variant
None
dsDNA
ssDNA
% GFP Positive
Nuclease:
None
Cas9
gRNA:
None
Off-Target
On-Target
E
Nuclease
None
Cas9
D10A Nickase
Template (RAB11A-GFP)
dsDNA
ssDNA
0.08%
24.2%
20.3%
0.00%
10.1%
4.5%
GFP
F
Nuclease + Template Combination
None
Cas9 + dsDNA
D10A + dsDNA
Cas9 + ssDNA
D10A + ssDNA
% GFP Positive
Nuclease:
None
Cas9 OR D10A
gRNA:
None
Off-Target
On-Target

Fig. 4. D10A nickase and ssDNA HDR templates reduce off-target integrations.
(A) Combinations of Cas9 RNPs and a RAB11A-GFP dsDNA HDR template were electroporated into primary human T cells. dsDNA template alone, or with an RNP containing a scrambled gRNA matching no sequence in the human genome yielded small but detectable amounts of GFP expression, which was noticeably increased when a dsDNA template is electroporated with a gRNA targeting a site different from the targeted RAB11A-GFP integration site (the "off-target RNP" targets *CXCR4* Exon 1). **(B)** Off-target integrations were consistently present in cells from different donors when the RAB11A-GFP dsDNA HDR template was electroporated with the off-target RNP, and fewer off-target integrations occurred when the dsDNA HDR template alone was electroporated. **(C)** Cas9 nuclease variants D10A (nickase) and inactive dCas9 significantly decreased off-target integrations when a single off-target *CXCR4* gRNA was used, but D10A nickase (with an "On-target" pair of gRNAs in a PAM-out orientation) led to efficient on-target integration of the *RAB11A* dsDNA HDR template. **(D)** Electroporation of a ssDNA HDR template reduced the off-target integrations to the limit of detection (comparable to levels with no template electroporated) both with no nuclease added and at induced off-target dsDNA breaks (Off-target gRNA + Cas9). **(E to F)** For integration of GFP fusion at the *RAB11A* site, use of a D10A nickase with a ssDNA HDR template reduced the on-target HDR (GFP integration with on-target gRNA) compared to Cas9 with a dsDNA template, but strongly reduced off-target integrations to undetectable levels. All fluorescent readouts were performed 4 days post-electroporation. Displayed data is representative of at least two different donors (A and E) or the averages of two different donors (C, D, and F) with standard deviation shown.

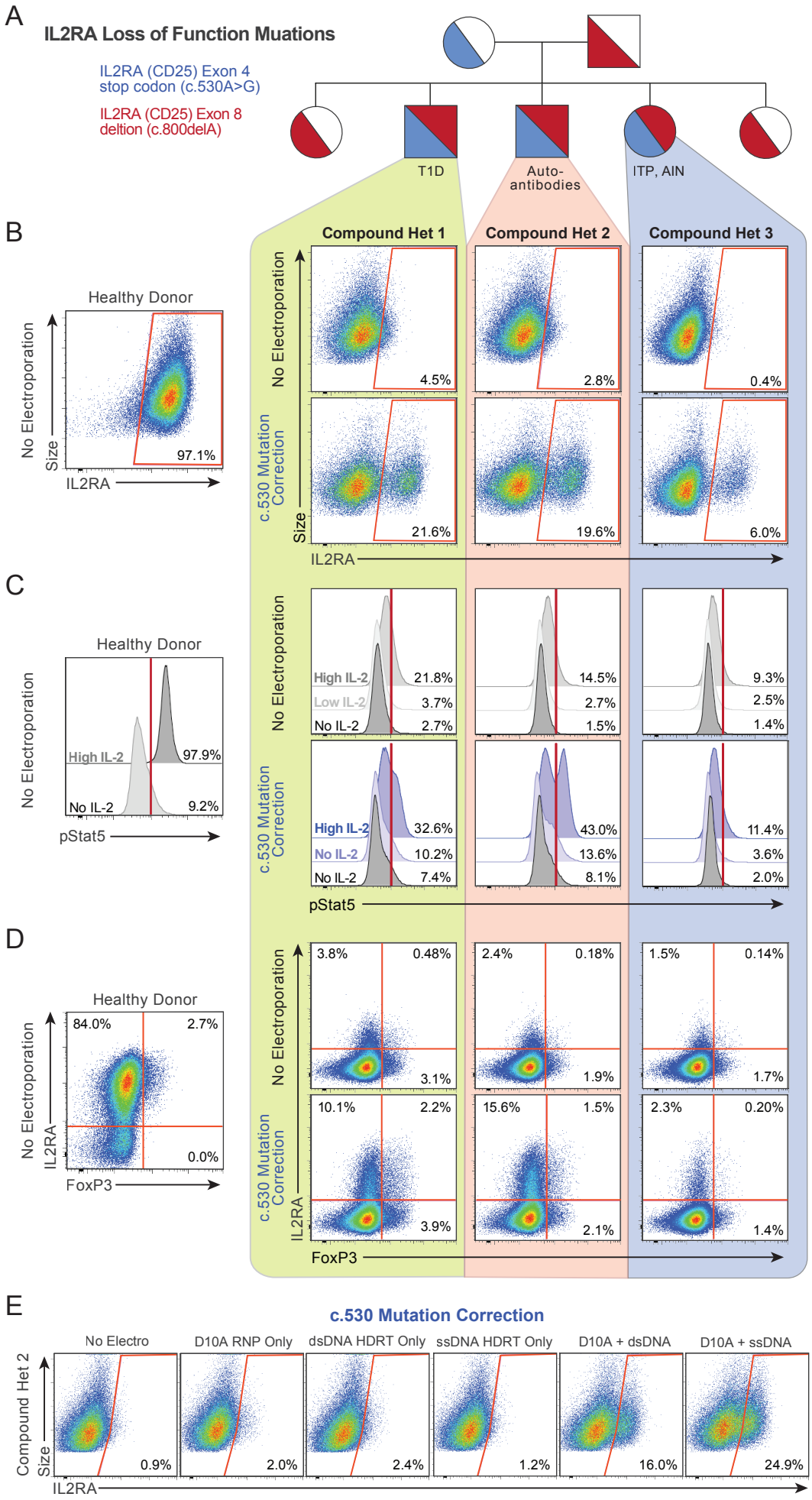
A
IL2RA Loss of Function Muations
IL2RA (CD25) Exon 4 stop codon (c.530A>G)
IL2RA (CD25) Exon 8 deltion (c.800delA)
T1D
Auto-antibodies
ITP, AIN
B
Healthy Donor
No Electroporation
Size
IL2RA
97.1%
Compound Het 1
Compound Het 2
Compound Het 3
No Electroporation
c.530 Mutation Correction
4.5%
2.8%
0.4%
21.6%
19.6%
6.0%
C
Healthy Donor
High IL-2
No IL-2
97.9%
9.2%
pStat5
Low IL-2
21.8%
3.7%
2.7%
14.5%
2.7%
1.5%
9.3%
2.5%
1.4%
32.6%
10.2%
7.4%
43.0%
13.6%
8.1%
11.4%
3.6%
2.0%
D
Healthy Donor
84.0%
2.7%
0.0%
FoxP3
3.8%
0.48%
3.1%
2.4%
0.18%
1.9%
1.5%
0.14%
1.7%
10.1%
2.2%
3.9%
15.6%
1.5%
2.1%
2.3%
0.20%
1.4%
E
c.530 Mutation Correction
No Electro
D10A RNP Only
dsDNA HDRT Only
ssDNA HDRT Only
D10A + dsDNA
D10A + ssDNA
Compound Het 2
0.9%
2.0%
2.4%
1.2%
16.0%
24.9%

Fig. 5. Monogenic autoimmune mutation corrected by non-viral gene targeting in primary human T cells

(A) Three siblings in a family carry two different *IL2RA* (encoding high-affinity IL-2 receptor, CD25) mutations (c.530A>G creating a stop codon in *IL2RA* exon 4; c.800delA, creating a frameshift mutation in *IL2RA* exon 8 which causes an almost 100 amino acid run-on). **(B)** These three compound heterozygote siblings show greatly reduced, but not completely absent, cell surface expression of IL2RA on their primary T cells. Non-viral gene targeting of the c.530 mutation by electroporation of a Cas9 RNP and a dsDNA HDR template containing the correct *IL2RA* sequence (along with a silent mutation in the targeted PAM sequence) successfully rescued IL2RA cell surface expression in a portion of T cells from each compound heterozygote sibling 2 days following electroporation. **(C)** 7 days after non-viral gene targeting, targeted T cells showed increased phosphorylation levels of Stat5 upon IL-2 stimulation compared to non-targeted controls. **(D)** 9 days following non-viral gene targeting to correct the c.530 mutation, IL2RA+ T cells from the three compound heterozygote donors include an increased level of FoxP3+ cells compared to non-targeted cells or healthy donor cells. **(E)** Non-viral gene targeting and correction of the c.530 mutation is possible and efficient using an optimized therapeutic reagent set (D10A nickase along with ssDNA HDR template). T cells from one compound heterozygote donor were stained for IL2RA surface expression after 9 days of *ex-vivo* expansion following electroporation (2 days following re-stimulation).

Table 1

Patient	Sex	IL2RA Mutation Status	Autoimmune Disease Phenotype	Clinical History	Autoantibodies
c.530 Het 1 (Mother)	F	c.530A>G / WT	None	Childhood ear infections	None
c.800 Het 1 (Father)	M	c.800delA / WT	None	No medical issues	None
c.800 Het 2	F	c.800delA / WT	None	Allergies	None
c.800 Het 3	F	c.800delA / WT	None	No medical issues	None
Comp Het 1	M	c.530A>G / c.800delA	Type 1 Diabetes	Insulin dependent diabetes in first year of life	anti-GAD, ICA512
Comp Het 2	M	c.530A>G / c.800delA	Diabetes Autoantibodies	Ear infections; Eczema	anti-GAD, MIAA, ICA
Comp Het 3	F	c.530A>G / c.800delA	Immune Thrombocytopenic Purpura; Autoimmune Neutropenia	Ear infections; Hemolytic anemia; Nummular dermatitis; Hypercellular bone marrow with inverted CD4/CD8 ratio; Mouth ulcers	anti-platelet

Table 1. Clinical history of family members with *IL2RA* mutations.
Mutation status and clinical phenotypes of members of a family with two separate *IL2RA* mutations, including three compound heterozygotes.